Genetic analysis of cis-enhancers associated with bone mineral density and periodontitis in the gene SOST

Avneesh Chopra
Department of Periodontology, Oral Medicine and Oral Surgery, Institute for Dental and Craniofacial Sciences, Charité-University Medicine Berlin

Jiahui Song
Department of Periodontology, Oral Medicine and Oral Surgery, Institute for Dental and Craniofacial Sciences, Charité-University Medicine Berlin

January Weiner 3rd
Core Unit Bioinformatics, Berlin Institute of Health

Dieter Beule
Core Unit Bioinformatics, Berlin Institute of Health

Arne S. Schaefer
arne.schaefer@charite.de

Department of Periodontology, Oral Medicine and Oral Surgery, Institute for Dental and Craniofacial Sciences, Charité-University Medicine Berlin

Article

Keywords: periodontitis, bone mineral density, SOST, causal variant, rs9783823, CEBPB

Posted Date: June 20th, 2024

DOI: https://doi.org/10.21203/rs.3.rs-4409923/v1

Additional Declarations: No competing interests reported.

Abstract

A haplotype block at the sclerostin (*SOST*) gene correlates with bone mineral density (BMD) and increased periodontitis risk in smokers. Investigating the putative causal variants within this block, our study aimed to elucidate the impact of linked enhancer elements on gene expression and to evaluate their role in transcription factor (TF) binding. Using CRISPR/dCas9 activation (CRISPRa) screening in SaOS-2 cells, we quantified disease-related enhancer activities regulating *SOST* expression. Additionally, in SaOS-2 cells, we investigated the influence of the candidate TFs CCAAT/enhancer-binding protein beta (CEBPB) on gene expression by antisense (GapmeR) knockdown, followed by RNA sequencing. The periodontitis-linked SNP rs9783823 displayed a significant cis-activating effect (25-fold change in *SOST* expression), with the C-allele containing a CEBPB binding motif (position weight matrix (PWM) = 0.98, $P_{corrected} = 7.7 \times 10^{-7}$). *CEBPB* knockdown induced genome-wide upregulation but decreased epithelial-mesenchymal transition genes (P = 0.71, AUC = 2.2×10^{-11}). This study identifies a robust *SOST* cis-activating element linked to BMD and periodontitis, carrying CEBPB binding sites, and highlights *CEBPB*'s impact on epithelial-mesenchymal transition.

Introduction

Bone remodeling is a process that adjusts the distribution of bone mass to meet multiple demands throughout life, including replacing damaged or old bone with new bone. To adapt bone mass to specific demands, cells integrate mechanical and metabolic environmental cues to balance bone formation and resorption (Bolamperti et al. 2022). Specifically, the loading of bone by dynamic mechanical forces is "sensed" by mature osteocytes within the mineralized matrix. Mechanical loading results in the suppression of the *SOST* gene, an inhibitor of the Wnt/β-catenin pathway specific to bone tissue, whereas bone unloading induces osteocytes to synthesize and secrete SOST, which promotes osteoclast genesis and results in reduced bone formation and bone mass loss (van Bezooijen et al. 2009). Thus, SOST is a negative regulator of bone formation. Similarly, numerous genome-wide association studies (GWAS) have shown genetic associations of *SOST* with BMD and fractures (Estrada et al. 2012; Kemp et al. 2017; Kichaev et al. 2019; Medina-Gomez et al. 2018; Morris et al. 2019; Styrkarsdottir et al. 2009; Surakka et al. 2020), and increased serum levels of SOST correlate with decreased BMD (Cejka et al. 2012; Sheng et al. 2012). In addition, GWAS have also reported genetic associations of *SOST* with high-density lipoprotein cholesterol and triglyceride levels (Hoffmann et al. 2018; Nielsen et al. 2020; Richardson et al. 2022; Surakka et al. 2015; van Leeuwen et al. 2016). Similarly, higher serum SOST levels correlate positively with serum triglyceride levels (Frysz et al. 2022). In addition, several GWAS have also found an association between *SOST* and blood eosinophil counts (Astle et al. 2016; Chen et al. 2020; Vuckovic et al. 2020), white blood cells whose functions include modulation of inflammatory responses as well as anti-parasitic and bactericidal activity. Similarly, a role for SOST in the control of inflammation has been reported in mouse models where SOST inhibited tumor necrosis factor alpha (TNFA)-induced innate immune responses (Donham et al. 2021; Wehmeyer et al. 2016). These findings suggest a more

complex role for SOST with a function in bone metabolism, but also in energy and inflammatory signaling (reviewed in (Fairfield et al. 2017).

SOST transcript and protein levels were also found to be significantly elevated in gingival tissue from patients with the oral inflammatory disease periodontitis (Napimoga et al. 2014), a complex common disease diagnosed by progressive alveolar bone loss as a result of oral inflammation (Lamont et al. 2018). Periodontitis has been epidemiologically associated with BMD in adolescents (Costa et al. 2021), young adults (Chou et al. 2021), and the elderly (Tezal et al. 2000). In a recent study, we found a common haplotype block in the genetic region of *SOST*, which was associated with BMD (rs1513670) (Styrkarsdottir et al. 2009) and severe periodontitis (classified as periodontitis stages III/IV, grade C; PIII-IV/C) diagnosed in young adults (rs6416905, linkage disequilibrium $r^2 > 0.8$) (Freitag-Wolf et al. 2019). Of note, the genetic association with periodontitis was found in a gene x smoking interaction study and only in tobacco smokers, resulting in an increased PIII-IV/C risk in smokers but not in nonsmokers. The common association of this haplotype block implies pleiotropic effects on BMD and periodontitis in smokers. Notably, tobacco smoking renders bone susceptible to osteoporosis by causing an imbalance in the mechanisms of bone turnover, resulting in lower bone mass and BMD, as recently reviewed (Al-Bashaireh et al. 2018).

Knowledge of the molecular genetic mechanisms underlying this common association would help to better understand the common etiology of the inflammatory and metabolic bone diseases periodontitis and osteoporosis. Therefore, this study aimed to find the putative causative variant(s) of this association and to identify the molecular mechanism contributing to the increased disease risk and mediating the putative impaired *SOST* regulation.

Materials and Methods

Screening for functional variants associated with periodontitis

LD ($r^2 > 0.8$) between the BMD GWAS lead SNP rs1513670, the periodontitis leads SNP rs6416905, and other common SNPs in this haplotype block was assessed using LDproxy (Machiela and Chanock 2015) with genotypes from the North-Western European populations CEU [Utah Residents with Northern and Western European Ancestry] and GBR [British in England and Scotland] (Genomes Project et al. 2010) from the International Genome Sample Resource (IGSR) (**Appendix Table 1**). We analyzed whether these SNPs were mapped to chromatin elements that correlate with regulatory functions of gene expression provided by ENCODE (ENCODE-Project-Consortium 2012) (Fig. 1). These elements were 1) open chromatin as determined by DNAse I hypersensitivity (DHS), 2) histone modifications H3K27Ac and H3K4Me1, 3) transcription factor binding sites (TFBS) experimentally confirmed by chromatin immunoprecipitation sequencing (ChIP-seq), and 4) chromatin state segmentation. We used the Transcription Factor Affinity Prediction (TRAP) Web Tools to bioinformatically determine whether the

SNP sequences of the associated variants contained conserved regulatory binding sites (Thomas-Chollier et al. 2011). We used the TRAP multiple sequence module with the vertebrate TF matrices from TRANSFAC and Jaspar and the 'human promoters' background model (Manke et al. 2008) with the reference and alternative allele SNP sequences as input and ranked the output by P value. In the exploratory screen, we set a multiple-test corrected P value threshold of $P < 5 \times 10^{-6}$ to reduce the number of false-positives. P values were corrected for multiple tests using the Benjamini-Hochberg method. We quantified the effects of the reference and alternative SNP alleles on the binding affinities of the TFs using the sTRAP software tool (Manke et al. 2010). The predicted TFBS that showed allele-specific differences in binding affinities were then manually checked for alignment of the SNP sequence with the specific TF motif, as indicated by the PWM. The matrix profiles for the predicted TFs were obtained from JASPAR (version 2022) (Castro-Mondragon et al. 2022). If the TF matrix profile was congruent with the DNA sequence at the SNP, a TF that showed significant binding sites at the SNP sequences as well as significant differences in binding affinities between the SNP alleles was considered indicative of a TF worthy of further molecular biological investigation.

Table 1
Top 10 up- and down-regulated protein-coding genes after *CEBPB* knockdown in SaOS-2 cells for 48 h.

	Gene	Entrez	Description	Log2FC	lfcSE	adj.P
up	*NOS3*	4846	nitric oxide synthase 3	11.314	1.185	5,90E-21
	ZNF560	147741	zinc finger protein 560	11.284	1.187	8,30E-21
	TUSC8	400128	tumor suppressor candidate 8	10,87	1.191	3,00E-19
	F13B	2165	coagulation factor XIII B chain	9.602	1.207	6,40E-15
	CERS3	204219	ceramide synthase 3	9.594	1.202	5,10E-15
	LRRC14B	389257	leucine rich repeat containing 14B	9.557	1.205	7,80E-15
	ANHX	647589	anomalous homeobox	9.437	0,651	1,10E-46
	CYP2C9	1559	cytochrome P450 family 2 subfamily C member 9	9.154	1.209	1,20E-13
	LDHAL6A	160287	lactate dehydrogenase A like 6A	9.043	1.214	3,20E-13
	RSPH10B2	728194	radial spoke head 10 homolog B2	8.982	1.213	4,30E-13
down	*KRT17*	3872	Keratin 17	-6.115	1.115	1,00E-07
	RAB7B	338382	member RAS oncogene family	-4.462	0,484	1,30E-19
	IL6	3569	Interleukin 6	-3.943	0,23	1,40E-64
	ARC	23237	activity regulated cytoskeleton associated protein	-3.907	0,196	3,60E-87
	CCNA1	8900	cyclin A1	-3.771	0,348	1,00E-26
	SLPI	6590	secretory leukocyte peptidase inhibitor	-3.742	0,622	4,90E-09
	ST8SIA6	338596	ST8 alpha-N-acetyl-neuraminide alpha-2,8-sialyltransferase 6	-3.535	0,628	4,50E-08
	C11orf86	254439	chromosome 11 open reading frame 86	-3.534	0,666	2,70E-07

	Gene	Entrez	Description	Log2FC	lfcSE	adj.P
	MEST	4232	mesoderm specific transcript	-3.417	0,584	1,30E-08
	IL2RB	3560	interleukin 2 receptor subunit beta	-3.387	0,319	1,40E-25

Cell culture and transfection

For CRISPRa experiments, HeLa cells were cultured as recently described (Chopra et al. 2021). HeLa cells were used because CRISPRa transfection can be efficiently performed in these cells and they have a high post-transfection survival rate. Briefly, cells were cultured in Earle's MEM medium containing 10% fetal bovine serum, 2 mM L-glutamine, 1% non-essential amino acids, and 1% penicillin-streptomycin. HeLa cells were seeded at 80,000 cells per 6-well (Techno Plastic Products, TPP) to achieve 50–60% confluence during transfection using jetPEI transfection reagent (Polyplus-transfection). For reporter gene assays, *CEBPB* knockdown, and overexpression experiments, we used the human bone osteosarcoma cell line SaOS-2, because in this osteoblast-like cell line, *SOST* is more highly expressed than in HeLa, suggesting that the transcriptional machinery, including TFs, that regulate *SOST* expression is present in this cell line. SaOS-2 cells were cultured in complete growth medium Alpha MEM Eagle (PAN-Biotech GmbH) supplemented with 10% fetal bovine serum and 50 mg/mL gentamicin. Prior to transfection with Lipofectamine 2000 (Thermo Fisher Scientific), SaOS-2 cells were seeded at 250,000 cells per well in a 6-well plate format for the reporter gene assays and *CEBPB* overexpression experiments. For the GapmeR knockdown experiment, SaOS-2 cells were seeded at a density of 100 cells per 6-well with Lipofectamine 2000 one day prior to GapmeRs (single-stranded antisense oligos) transfection.

Electrophoretic mobility shift assay (EMSA)

To determine allele-specific TF binding to the SNP DNA sequence, we performed EMSAs using the Gelshift Chemiluminescent EMSA Kit (Active Motif) as recently described (Chopra et al. 2021). Briefly, double-stranded oligonucleotides for each SNP allele, flanked by 21 bp up- and downstream in 3'-biotinylated and unbiotinylated forms, were obtained by annealing with their respective complementary primers (**Appendix Table 2**). Nuclear protein extract was prepared from SaOS-2 cells using the NE-PER Nuclear and Cytoplasmic Extraction Kit (Pierce Biotechnology). For supershift EMSA, 20 fmol of biotin-labeled oligonucleotide probes were incubated with 10 µg of nuclear protein extract in 1x binding buffer and 2 µL (10 µg/50 µL) of a specific monoclonal antibody (C/EBP beta (H-7): sc-7962; GFI-1 (B-9): sc-376949, both from Santa Cruz Biotechnology, Inc.) for 20 min at room temperature. To verify the specific DNA-protein interaction, 4 pmol of unlabeled oligonucleotides were added to the binding reaction. The DNA-protein complexes were electrophoresed in a 5% native polyacrylamide gel in 0.5x TBE buffer at 100 V for 1 h and visualized by chemiluminescence detection (Chemostar Touch, INTAS) after electrotransfer and crosslinking of the products on a nylon membrane. Band intensities were quantified by the absolute value area of the shifted antibody bands using the ImageJ software (Rueden et al. 2017).

Table 2
Top Enriched Gene Sets after 48 h CEBPB knockdown in SaOS-2 cells.

Gene Set Collection	ID	Title	Gene Number	AUC	adj.P
Hallmark	M5930	EPITHELIAL MESENCHYMAL TRANSITION	190	0,74	3,60E-40
KEGG	M7098	ECM RECEPTOR INTERACTION	71	0,73	1,60E-12
Reactome	M27218	NON INTEGRIN MEMBRANE ECM INTERACTIONS	55	0,71	2,70E-09
tmod	LI.M2.0	ECM (I)	30	0,77	5,30E-07
GO	M12343	REGULATION OF SUBSTRATE ADHESION DEPENDENT CELL SPREADING	51	0,71	1,40E-06

Luciferase-based reporter gene assays

The DNA sequences spanning the putative causal SNPs were cloned into the firefly luciferase vector pGL4.24 (Promega) to subsequently test their regulatory potential on reporter gene expression. The reporter gene plasmids containing either the reference or alternative allele within the TF binding motif differed by a single nucleotide and were amplified by PCR. Primer sequences are listed in **Appendix Table 3**. The PCR products were inserted into the *Hin*dIII restriction site of the reporter plasmids upstream of the minimal promoter. Reporter plasmids were amplified in 5-alpha competent *E. coli* (NEB) and extracted using the QiaPrep Plasmid Mini Kit (Qiagen).

SaOS-2 cells were co-transfected in triplicates with 2.7 µg firefly luciferase reporter plasmid carrying the allele-specific SNP sequence together with 0.3 µg *renilla* luciferase reporter vector phRL-SV40 (Promega) in 6-well plates. As controls, SaOS-2 cells were transfected with the empty pGL4.24 and phRL-SV40 plasmids. After 24 hours, firefly and *renilla* luciferase activities were quantified using the Dual-Luciferase Stop & Glo Reporter Assay System (Promega) with a luminometer (Orion II Microplate, Berthold). Reporter plasmid activities were quantified as relative light units and normalized as the ratio of luciferase to *renilla* activity to calculate relative fold changes. Differences in transcript levels were calculated using a two-sided T-Test with GraphPad Prism 6 software (GraphPad Software, Inc.).

CRISPR/dCas9 activation (CRISPRa) & quantitative real-time PCR (qRT-PCR)

Assigning the regulatory effects of associated regions on specific genes based on public eQTL data and linear proximity to the nearest gene is prone to error, as eQTLs are statistical observations without direct molecular evidence (Zeng et al. 2017), and enhancers are often mapped at great distances from their actual targets and do not necessarily affect the expression of the nearest gene. Induction of *SOST*

expression by positioning an activator protein at the sites of the associated SNPs using the CRISPRa system allows quantification of the effects of putative enhancers on *SOST* expression and provides direct evidence of cis-regulatory function. CRISPRa allows specific and efficient quantification of the regulatory potential of a genomic sequence on the expression of candidate target genes at physiological concentrations and in the endogenous chromosomal context including naturally occurring genetic variants (Simeonov et al. 2017). Therefore, we used CRISPRa to analyze whether the associated regions have cis-regulatory effects on *SOST* expression. To test cis-regulatory effects, we aligned the 36 linked haplotype SNPs to the chromosomal locations and integrated chromatin elements from ENCODE (ENCODE-Project-Consortium 2012) that correlate with regulatory functions of gene expression characterized by DNAse I hypersensitivity, H3K4Me1 methylation, and TF ChIP-Sequencing clusters determined by the ENCODE 3 project (Davis et al. 2018) (Fig. 1). We designed 9 sgRNAs to target the putative regulatory elements in the intergenic region downstream of *SOST*, which carried the linked SNPs. 4 sgRNAs were designed to target the promoter region of *SOST*, which also carried linked SNPs. SgRNAs were designed using the E-CRISP online tool (Heigwer et al. 2014). A scrambled sgRNA with no genomic target was used as a negative control, as described in (Chopra et al. 2021). The *SOST* sgRNAs and chromosomal locations are listed in the **Appendix Table 4**. For CRISPRa of *GFI-1*, we used the best-functioning sgRNA (fw (5'-3'): CACCGCAAAATTAAAGGCCGCGCGG; rev (5'-3'): AAACCCGCGCGGCCTTTAATTTTGC) targeting the *GFI-1* promoter upstream of -70 transcription start site (TSS).

We cloned the sgRNA sequences into the sgRNA(MS2) vector (plasmid #61424) at the *Bbs*I site according to the protocol described in (Ran et al. 2013). The CRISPRa system was transfected into HeLa cells. For CRISPRa, each 6-well was transfected with 1 µg sgRNAs(MS2) (containing specific sgRNA(s)), 1 µg dCAS9-VP64_GFP [plasmid #61422], and 1 µg MS2-P65-HSF1_GFP [plasmid #61423] and incubated for 44 h. All plasmids were obtained from Addgene (cloning backbone plasmids was a gift from Feng Zhang) (Konermann et al. 2015). For quantitative analysis of specific CRISPRa, we used qRT-PCR. Total RNA was extracted from human cells using the RNeasy Mini Kit (Qiagen) according to the manufacturer's instructions. Complementary DNA (cDNA) was synthesized from 500-1,000 ng DNA-free total RNA, using the High-Capacity cDNA Reverse Transcription Kit (Applied Biosystems). SYBR Select Master Mix (Applied Biosystems) was used with the following primers: *GAPDH: 5'-CAAATTCCATGGCACCGTCA-3', 5'-CCTGCAAATGAGCCCCAG-3', SOST: 5'-GCTGGAGAACAACAAGACCA-3', 5'-GTAGCGGGTGAAGTGCAG-3', CEBPB: 5'-AGCGACGAGTACAAGATCCG-3', 5'-AGCTGCTCCACCTTCTTCTG-3', GFI-1: 5'-CCGCGCTCATTTCTCGTCA-3', 5'-ACGGAGGGAATAGTCTGGTCC-3'.* Relative fold changes in gene expression were calculated by the $2^{-\Delta\Delta Ct}$ method with *GAPDH* as the reference gene. Statistical differences in transcript levels were calculated using a T-Test.

Sequencing of rs9783823 in IMR90 and A549 cells

DNA was extracted (Blood & Cell Culture DNA Mini Kit, Qiagen) from cell pellets of IMR90 and A549 cells provided by Prof. Clemens Schmidt, Cancer Genetics and Cellular Stress Responses Group, Max Delbrück Center for Molecular Medicine (MDC), Berlin, Germany. A region up and downstream of

rs9783823 was amplified by PCR (5'-CGAGTCTCACTTCCTACCTCA-3', 5'-AGAATCACCTGGAGAGCTGT-3'), and the 279 bp PCR product was sequenced in both directions by the Sanger method at LGC Genomics, Berlin.

CEBPB knockdown in SaOS-2 cells and RNA sequencing

LNA GapmeRs either targeting unique regions of *CEBPB* isoforms or not targeting any region (scrambled, used as negative control) were designed by Qiagen. A mixture of 3 LNA GapmeRs or one scrambled LNA GapmeR was used. The GapmeRs hybridized to unique regions of *CEBPB* isoforms as follows: Gene Globe ID LG00828145-DDA, LG00828146-DDA, LG00828147-DDA. LNA GapmeRs were transfected into SaOS-2 cells at a final concentration of 225 µM for 48 h. Total RNA was extracted using the RNeasy Mini Kit (Qiagen, Germany). 500 ng total RNA from transfected cell cultures were sequenced on a NextSeq 500 with 16 million reads (75 bp single end) using the NextSeq 500/550 High Output Kit v2.5 (75 cycles). RNA sequencing was performed at the Berlin Institute of Health, Core Facility Genomics. Reads were aligned to the human genome sequences (build GRCh38.p7) using the STAR aligner v. 2.7.8a (Dobin et al. 2013). Quality control (QC) of the reads was inspected using the multiqc reporting tool (Ewels et al. 2016), which combines several approaches, including fastqc (available online at http://www.bioinformatics.babraham.ac.uk/projects/fastqc), dupradar (Sayols et al. 2016), qualimap (Garcia-Alcalde et al. 2012), and RNA-SeqC (DeLuca et al. 2012). Raw counts were extracted using the STAR program. Differential gene expression was performed using the R package DESeq2 (Love et al. 2014), and version 1.30 was used. Gene set enrichment was performed with the CERNO test from the tmod package (Zyla et al. 2019), version 0.50.07, using the gene expression profiling-based gene set included in the package, and MSigDB (Liberzon et al. 2015), v.7.4.1. The goseq package, version 1.38 (Young et al. 2010), was used for the hypergeometric test and the Gene Ontology gene sets. The P values of differentially expressed genes were corrected for multiple tests using the Benjamini-Hochberg correction. The corrected P values are given as q values (false discovery rate [FDR]).

CEBPB overexpression in SaOS-2 cells

CEBPB isoforms LAP2 and LIP were overexpressed in SaOS-2 cells using episomal expression plasmids (pCMV-FLAG LAP2 (#15738); pCMV-FLAG LIP (#15737)) to determine whether *CEBPB* affects *SOST* expression. These plasmids were obtained from Addgene (gifted from Joan Massague). To normalize the overexpression experiment, the empty pGL4.24 vector was used as a control plasmid. 3 µg of each vector was transfected into SaOS-2 cells and incubated for 48h, followed by RNA extraction and qRT-PCR.

Results

CRISPRa screen identifies strong cis-regulatory elements downstream of SOST associated with alveolar bone loss

SNPs rs1513670 and rs6416905 were lead SNPs showing an association with BMD and periodontitis in smokers (Freitag-Wolf et al. 2019; Styrkarsdottir et al. 2009). These two SNPs were in strong LD ($r^2 > 0.8$) with each other and with 34 additional SNPs (**Appendix Table 1**), spanning the transcribed region of *SOST*, including a large intergenic region downstream of the 3'UTR (Fig. 1). We first identified disease-associated regulatory cis-regulatory chromatin elements that are in strong LD with the associated SNPs. To this end, we transfected HeLa cells with the CRISPRa system, which encodes sgRNAs designed to direct the SAM activation system to chromatin elements that exhibit biochemical enhancer marks such as DHS, H3K27Ac, and H3K4Me1 histone modifications, as well as TFBS experimentally confirmed by ChIP-Seq (provided by ENCODE; Fig. 1). We chose HeLa cells because this cell line allows efficient CRISPRa plasmid transfection and does not show *SOST* expression according to the Human Protein Atlas (https://www.proteinatlas.org/ENSG00000167941-SOST/cell+line).

The strongest induction of *SOST* expression was observed with sgRNAs targeting the *SOST* promoter 270 bp and 1,100 bp upstream of the TSS, with a 5,119-fold and 56-fold increase in *SOST* expression, respectively. This demonstrated the functionality of our CRISPRa system to induce *SOST* expression. An associated enhancer located 12.9 kb downstream of the *SOST* 3'UTR showed a 25-fold increase in *SOST* transcript levels. The second strongest associated enhancer showed a 5-fold increase in expression and was located 11.6 kb downstream of the *SOST* 3'UTR. H3K27Ac marks were most prominent in these regions (ENCODE) (Fig. 1**)**. The other predicted enhancers marked by associated SNPs showed a < 3-fold increase in *SOST* expression. These regions showed much weaker biochemical marks of active regulatory elements or no enhancer marks.

Bioinformatic analysis of associated SNPs predicts allele-specific effects on TF CEBPB and GFI-1 binding affinities in functional cis-regulatory elements

14 associated SNPs in strong LD ($r^2 > 0.8$) were located on the enhancer shown in our CRISPRa screen to have the strongest cis-regulatory effect on *SOST* expression. To identify biologically functional SNPs, we analyzed whether the different alleles of these 14 SNPs have any predicted effects on the binding affinities of TFs (**Appendix Table 1**). The highest-ranked TFBS was found for rs9783823 (**Appendix Table 5**). This SNP was predicted to bind CEBPB ($P_{combined} = 7.7 \times 10^{-7}$, PWM = 0.98). The CEBPB motif was predicted to have strong binding affinity on the reference C-allele ($P < 3.29 \times 10^{-6}$), but not on the alternative T-allele (P = 0.013). The ancestral (reference) rs9783823-C allele of the CEBPB motif was less common in European populations (C = 0.398 EUR) compared to African populations (C = 0.608 AFR). TF ChIP-Seq clusters (338 factors, 130 cell types) from ENCODE 3 also showed binding of CEBPB in the native human chromatin in this region. ENCODE reported 2 CEBPB ChIP-Seq peaks at chr17:41810335–41810590 (hg19) (peak 1) and chr17:41811788–41812043 (peak 2). These data were taken from ENCODE, which was generated in cultured white Caucasian lung fibroblasts (IMR90 and A549 cells) (**Appendix Material**). The CEBPB binding motifs at peak 1 and peak 2 were predicted with P < 0.00041 and P < 0.00083 (CEBPB motif +/- 5bp), respectively. The C-allele of the CEBPB binding sites at peak 1 and peak 2 are located at chr17:41810515 and chr17:41811942 (hg19), respectively. The rs9783823-C

allele at the CEBPB binding site is located at chr17:41813369. Notably, this resulted in a distance of exactly 1,427 bp between the C-alleles of the CEBPB motifs of ChIP-Seq peaks 1 and 2, and also 1,427 bp between the C-alleles of the CEBPB motifs of ChIP-Seq peak 2 and rs9783823. We next investigated the possible reason for the absence of a CEBPB-specific ChIP-Seq peak at rs9783823. The lung fibroblast cell lines IMR90 and A549 were derived from white Caucasians. In this genetic ancestry, the reference allele rs9783823-C of the CEBPB motif is the minor allele (C|C = 0.155, C|T = 0.485, and T|T = 0.360; EUR population, ENSEMBL). We sequenced rs9783823 in IMR90 and A549 cells and found that both cell lines were homozygous for rs9783823-T (**Appendix Fig. 1**), indicating a loss of the CEBPB motif. In addition, our TFBS analysis revealed a conserved regulatory binding site of the transcriptional repressor GFI-1 for SNP rs8071941 (P = 0.002) and a predicted difference in binding affinity between the two alleles of log(P) = -3.14. The TFBS prediction was not significant after correction for multiple testing and did not pass the pre-assigned significance threshold of p < 5 x 10E-6. However, the DNA sequence at rs8071941 matched the GFI consensus binding motif, and the GFI-1 binding site of SNP rs8071941 was located on CEBPB ChIP-Seq peak 1, 195 bp upstream of the C-allele of the CEBPB motif. Subsequently, we also searched the DNA sequence of peak 2 for GFI-1 binding sites and observed a second GFI-1 binding site on ChIP-Seq peak 2, 81 bp upstream of the C-allele of CEBPB. GFI-1 binding at this site was predicted by TRAP with P < 0.0014 (observed GFI-1 motif +/- 5 bp; rank 1). On this enhancer region, we found no other TF motif with significantly different binding affinities between an associated SNP allele and the congruence of the predicted TF motif and the DNA sequence of the SNP. The enhancer (chr17:41816483–41820007, 3.525kb; hg19) that showed the second strongest cis-regulation of *SOST* in our CRISPRa screen had 3 associated SNPs (rs2076793, rs9303540, and rs9908933). These SNPs did not show TFBS with predicted differences in binding affinities between the two SNP alleles with a match of the DNA sequence of the SNPs and the TF motif.

rs9783823-T impairs TF CEBPB binding

To validate the predicted CEBPB binding at rs9783823, we performed EMSAs with CEBPB antibody and rs9783823 allele-specific DNA probes using nuclear protein extract from SaOS-2 cells. In this cell line, *CEBPB* is moderately expressed (nTPM = 30.4; Human Protein Atlas). The binding of CEBPB antibodies to probes specific for the T-allele of rs9783823 reduced CEBPB binding by 14–23% compared to probes with the C-allele (Fig. 2, **Appendix Fig. 2**).

We then investigated whether the alleles at rs9783823 affect gene activity using luciferase reporter genes in SaOS-2 cells. In the background of the rs9783823 C-allele, reporter luciferase activity was 3.8-fold higher compared to the T-allele (P < 0.0001). The rs9783823-C allele increased luciferase activity 2.3-fold compared to the empty plasmid (P < 0.0001), whereas the alternative T-allele showed no increase in luciferase activity (-1.5-fold; Fig. 3). Consistent with our experiments, the GTEx data also indicated that rs9783823 is a biologically functional SNP that correlated with regulatory effects on *SOST* expression. GTEx observed that rs9783823 had the strongest eQTL effect on *SOST* expression compared to other genes, with reduced *SOST* expression in the genetic background of the T-allele (normalized effect size β = -0.17, P = 5.1 x 10^{-13}; observed in the artery.

CEBPB knockdown represses genes involved in epithelial-mesenchymal transition and extracellular matrix (ECM) interaction in SaOS-2 cells

CEBPB mutant mouse strains showed delayed bone formation with suppression of osteoblast differentiation (Tominaga et al. 2008). *CEBPB* loss-of-function mice showed increased bone resorption and dysregulated expression of *CEBPB* affects bone mass (Smink et al. 2009). Therefore, we were interested in investigating the effects of *CEBPB* knockdown in SaOS-2 cells. Silencing *CEBPB* expression in SaOS-2 cells using a mixture of 3 LNA GapmeRs resulted in a 64% reduction of *CEBPB* expression (determined by qRT-PCR, Fig. 4A). Genome-wide expression profiling by RNA-Seq after *CEBPB* knockdown using a mixture of 3 LNA GapmeRs revealed 3,787 upregulated genes with $\log_2$ fold change ($\log_2$FC) ≥ 2) and 604 downregulated genes with $\log_2$FC < -1 ($P_{adj} < 0.05$; Fig. 4B**).** The most upregulated protein-coding gene with the lowest P value was the gene *nitric oxide synthase 3* (*NOS3*) ($\log_2$FC = 11.31, $P = 6 \times 10^{-21}$) and the most downregulated protein-coding gene was the gene *keratin 17* (*KRT17*) ($\log_2$FC = -6.1, $P = 4 \times 10^{-8}$; Table 1). Using qRT-PCR, we observed a weak increase, however not significant, of *SOST* relative transcript levels (Fig. 4C). Our RNA-Seq data showed that *CEBPB* knockdown correlated with a weak increase in *SOST* expression ($\log_2$FC = 0.79) with $P_{adj} = 4.7^{-26}$ (Fig. 4D).

We performed gene set enrichment analysis (GSEA) with the co-expression gene set tmod and the Molecular Signatures Database (MSigDB) gene sets Reactome, Hallmark, KEGG, and GO, contrasting *CEBPB* knockdown cells to negative control transfected cells. The largest gene set of the gene set collections, which passed the significance threshold of $P_{adj} < 0.05$ and an area under the curve (AUC) > 0.7 indicated agonistic functions of *CEBPB* in the regulation of epithelial-mesenchymal transition and ECM interaction with AUC = 0.74 and $P_{adj} = 3.6 \times 10^{-40}$ (Table 2, Fig. 5, **Appendix Fig. 3)**.

CEBPB does not activate SOST expression in SaOS-2 cells

CEBPB knockdown did not reduce *SOST* expression (Fig. 4C**)**, suggesting that *CEBPB* does not activate *SOST* expression. This is in contrast to our reporter gene experiment and GTEx data. As a next step, we asked whether the upregulation of *CEBPB* would affect the activation of *SOST* expression. The *CEBPB* gene encodes 2 functional isoforms (designated liver-enriched activating proteins LAP1 and LAP2) and the N-terminal truncated form liver-enriched inhibitory protein LIP, which lacks transactivation domains and is thought to inhibit the functions of LAP by competitively binding to the same DNA recognition sites (Descombes and Schibler 1991). To test whether LAP and LIP isoforms affect *SOST* expression, we overexpressed LAP2 and LIP in SaOS-2 cells for 48 h using episomal expression plasmids. LAP2 and LIP expression were upregulated 137- and 319-fold, respectively. Overexpression of the functional *CEBPB* isoform LAP2 showed a significant reduction of relative transcript levels, whereas overexpression of the truncated *CEBPB* isoform LIP did not induce changes in *SOST* expression (Fig. 6A). This correlated with the results from *CEBPB* knockdown, which weakly induced *SOST* expression.

GFI-1 does not activate SOST expression in Hela cells

We tested whether *GFI-1* upregulation would affect *SOST* expression in Hela cells using CRISPRa. sgRNAs targeting the *GFI-1* promoter resulted in a 43-fold increase in *GFI-1* transcript levels. However, we observed no corresponding change in *SOST* transcript levels (Fig. 6B).

Discussion

In the current study, we identified the C-allele of rs9783823 as a biologically functional variant that impairs the binding of the TF CEBPB, with a putative causal contribution to increased alveolar bone loss of PIII-IV/C in smokers and reduced BMD. GTEx data showed that the rs9783823-C allele is significantly associated with increased *SOST* expression. Our data showed increased CEBPB binding in the background of the rs9783823-C allele as well as increased reporter gene expression, implying the functionality of this SNP. In addition, ChIP-Seq data from ENCODE confirmed CEBPB binding in this region in native chromatin and found 2 CEBPB ChIP-Seq peaks. We were able to show that IMR90 and A549 cells are homozygous for the T-allele of rs9783823, which explains the absence of a CEBPB ChIP-Seq peak at rs9783823. Remarkably, we found that the distance of the C-allele of the CEBPB motif at rs9783823 is identical to both ChIP-Seq peak 1 and peak 2, each with a distance of 1,427 bp. This suggests a possible stereometric function of the 3 CEBPB motifs. In general, only a small fraction of the sites for a given TF are bound by that TF, and this binding depends in part on the surrounding 3D environment (Dror et al. 2015), which may be reflected in the identical spacing of the three CEBPB binding sites. Taken together, these data suggest a role for CEBPB in the regulation of *SOST* expression. However, the upregulation of LAP2 in SaOS-2 cells did not alter *SOST* expression. This could be due to the strong baseline expression of *CEBPB* in SaOS-2 cells, which implies an a priori saturation of CEBPB binding sites. The ancestral allele of rs9783823 is C (C = 0.608 AFR) and the alternative allele is T. This implies a C ◊ T transition. Those transitions occur spontaneously in the genome by oxidative deamination of 5-methylcytosine (5mC) to thymine (T). In most cases the resulting T:G mismatches are repaired. However, C:T mutations are enriched in the binding sites of CEBP, and it has been shown that within a CEBP site, the presence of a T:G mismatch increases the binding affinity of CEBP by a factor of > 60 compared to the normal C:G base pair (Yang et al. 2021). It has been suggested that this increased binding of CEBP to the T:G mismatch inhibits its repair. The passage of a replication fork over a T:G mismatch before repair can occur results in a C-to-T mutation in one of the daughter duplexes, providing a plausible mechanism for the accumulation of C-to-T somatic mutations in humans. In this context, the C and T alleles at rs9783823 indicate a CEBPB footprint of this TFBS, implying a biologically functional ancient CEBPB motif at this site. Our GSEA revealed that *CEBPB* knockdown repressed genes involved in epithelial-mesenchymal transition and ECM interaction. This suggests that CEBPB has an activating effect on these functions. This is consistent with previous studies that showed, for example, that knockdown of *CEBPB* in TNBC cells resulted in downregulation of genes involved in cell migration, extracellular matrix production, and cytoskeletal remodeling, many of which were epithelial-to-mesenchymal transition (EMT) marker genes (Sterken et al. 2022). In addition, CEBPB was identified as a master regulator of the mesenchymal phenotype, and overexpression of *CEBPB* in neural stem cells caused loss of neuronal differentiation, manifestation of a fibroblast-like morphology, induction of

mesenchymal genes, and enhanced migration in a wound assay (Carro et al. 2010). Conversely, siRNA- and shRNA-mediated *CEBPB* knockdown in SNB19 GBM cells showed suppression of the mesenchymal signature. At the single gene level, we observed that *CEBPB* knockdown correlated with a strong reduction of *KRT17* and *IL6* expression. This observation was also inconsistent with previous studies, which reciprocally showed that high *CEBPB* expression correlated with *KRT17* expression and the enhancer of this gene is regulated by CEBPB (Jinesh et al. 2018), and that overexpression of *CEBPB* resulted in a 10-12-fold increase in IL-6 production (Hungness et al. 2002). Our RNA sequencing data also showed that *CEBPB* knockdown was correlated with significantly reduced *SOST* expression. This supported our reporter gene data showing that CEBPB binding correlates with increased *SOST* expression. Notably, our RNA sequencing data showed that silencing of *CEBPB* correlated with ~ 6 times more upregulated genes than downregulated genes. However, our GSEA did not reveal any significant enrichment of a gene set of upregulated genes. Instead, we found several downregulated gene sets of genes known to be regulated by *CEPBP*, such as epithelial-mesenchymal transition and ECM receptor interactions. We speculate that the detection of significantly downregulated gene sets as well as downregulated individual genes, some of which are already known targets of *CEBPB* regulation, indicate the true effects of *CEBPB* repression. In contrast, the comparatively higher number of genes with higher expression, paralleled by the lack of enriched gene sets after *CEBPB* repression, is likely due to indirect effects and possibly an associated perturbation of natural cell function. These non-physiological effects would explain the lack of enriched upregulated gene sets. In particular, we hypothesized that CEBPB would positively regulate *SOST* because our reporter gene experiments as well as the GTEx data implied higher gene expression in the background of rs9783823-C allele, which is the CEBPB binding allele. However, in our RNA sequencing data, we did not detect a downregulation of *SOST* after *CEBPB* knockdown, but a weak upregulation. Consistent with our interpretation that weakly upregulated genes in our RNA sequencing experiment reflect perturbation of natural cell function and are thus artifacts, we conclude that *CEBPB* does not positively regulate *SOST* expression in SaOS-2 cells. Therefore, we do not consider rs9783823 to be the causal variant of the association.

We also found a predicted conserved regulatory binding site of the transcriptional repressor GFI-1 at SNP rs8071941. It has previously been shown in knockout mice that loss of GFI-1 and housing under non-sterile conditions increases inflammatory response and bone mass loss (Geissler et al. 2018). In addition, GTEx showed that the GFI-1-binding rs8071941-A allele reduced *SOST* expression compared to the non-GFI-1-binding rs8071941-G allele (P = 5 x E-7, lung), consistent with the known repressor effect of GFI-1. However, we did not observe any effect of *GFI-1* overexpression on *SOST* expression after CRISPRa in SaOS-2 cells. Furthermore, GFI-1 binding to the genetic region of *SOST* has not yet been demonstrated by ChIP-Seq experiments from ENCODE and others (Helness et al. 2021; Sun et al. 2022). Moreover, GFI-1 knockout mice showed reduced *SOST* expression (Geissler et al. 2018), which is inconsistent with the effect of GFI-1 as a repressor of *SOST*. Taken together, we conclude that the causal variant of the haplotype block associated with periodontitis and BMD was not detected in this study.

A limitation of our study was that we did not examine all pleiotropic periodontitis- and BMD-associated SNPs, but limited the analyses to those SNPs that mapped to regulatory chromatin elements. Therefore,

causal variants may be located in other regions of the LD block. However, TFBSs generally localize to active chromatin, as reliably detected by DHS, H3K27Ac, and H3K4Me1 histone modifications, as well as TFBSs experimentally confirmed by ChIP-seq. The results of our CRISPRa screen were consistent with this, showing the strongest gene expression in the promoter, followed by the nominated strong enhancer, while the nominated weak enhancer and chromatin not indicated as an active enhancer by these biochemical modifications had weak or no effect, respectively. Alternatively, the effect alleles do not necessarily have to alter TFBS to modulate gene transcription. However, we did not find SNPs in LD with periodontitis and BMD-associated haplotype block located in the 5' or 3' UTRs or at splice sites that could modulate gene transcription. In addition, we found no nonsynonymous SNP in an exon that would alter protein function. To identify the causal sequences underlying the association, deletion experiments of regions of the enhancer carrying the associated SNPs would be required.

In conclusion, we have identified an enhancer with strong cis-regulatory effects on *SOST* expression. This enhancer carries the CEBPB TFBS as determined by ChIP-Seq data from ENCODE. rs9783823 is flanked by 2 CHIP-Seq CEBPB binding sites and is likely to be a CEBPB binding site based on the spacing and G:T conversion. Regulation of *SOST* by CEBPB and GIF-1 has not been demonstrated.

Declarations

Author Contribution

Study design: A.C., J.S., and A.S.; Methods and analysis: A.C., J.S., J.W., D.B., and A.S.; Interpretation of results: A.C., J.S., and A.S.; Drafting of the manuscript: A.C., J.S., and A.S.; Critical review of the manuscript: A.C., J.S., and A.S.; The authors declare no potential conflicts of interest regarding the authorship and/or publication of this article. All authors gave final approval and agreed to be accountable for all aspects of the work.

Acknowledgement

We thank Prof. Dr. Clemens Schmidt, Division of Cancer Genetics and Cellular Stress Responses, Max Delbrück Center for Molecular Medicine (MDC), Berlin, Germany, for providing cell pellets of IMR90 and A549 cells for sequencing. This work was performed with merit-based funding to A.S. from the Faculty of Medicine, Charité - Universitätsmedizin Berlin.

Data Availability

The data that support the findings of this study are available on request from the corresponding author. RNA-Seq data: Reads, raw counts, and the results of the differential expression analysis have been submitted to the Short Read Archive via the Gene Expression Omnibus (GEO accession number GSE269019).

References

1. Al-Bashaireh AM, Haddad LG, Weaver M, Chengguo X, Kelly DL, Yoon S. 2018. The effect of tobacco smoking on bone mass: An overview of pathophysiologic mechanisms. J Osteoporos. 2018:1206235.
2. Astle WJ, Elding H, Jiang T, Allen D, Ruklisa D, Mann AL, Mead D, Bouman H, Riveros-Mckay F, Kostadima MA et al. 2016. The allelic landscape of human blood cell trait variation and links to common complex disease. Cell. 167(5):1415–1429 e1419.
3. Bolamperti S, Villa I, Rubinacci A. 2022. Bone remodeling: An operational process ensuring survival and bone mechanical competence. Bone Res. 10(1):48.
4. Carro MS, Lim WK, Alvarez MJ, Bollo RJ, Zhao X, Snyder EY, Sulman EP, Anne SL, Doetsch F, Colman H et al. 2010. The transcriptional network for mesenchymal transformation of brain tumours. Nature. 463(7279):318–325.
5. Castro-Mondragon JA, Riudavets-Puig R, Rauluseviciute I, Lemma RB, Turchi L, Blanc-Mathieu R, Lucas J, Boddie P, Khan A, Manosalva Perez N et al. 2022. Jaspar 2022: The 9th release of the open-access database of transcription factor binding profiles. Nucleic Acids Res. 50(D1):D165-D173.
6. Cejka D, Jager-Lansky A, Kieweg H, Weber M, Bieglmayer C, Haider DG, Diarra D, Patsch JM, Kainberger F, Bohle B et al. 2012. Sclerostin serum levels correlate positively with bone mineral density and microarchitecture in haemodialysis patients. Nephrol Dial Transplant. 27(1):226–230.
7. Chen MH, Raffield LM, Mousas A, Sakaue S, Huffman JE, Moscati A, Trivedi B, Jiang T, Akbari P, Vuckovic D et al. 2020. Trans-ethnic and ancestry-specific blood-cell genetics in 746,667 individuals from 5 global populations. Cell. 182(5):1198–1213 e1114.
8. Chopra A, Mueller R, Weiner J, 3rd, Rosowski J, Dommisch H, Grohmann E, Schaefer AS. 2021. Bach1 binding links the genetic risk for severe periodontitis with st8sia1. J Dent Res.220345211017510.
9. Chou HH, Lu SL, Wang ST, Huang TH, Chen SL. 2021. The association between bone mineral density and periodontal disease in middle-aged adults. Int J Environ Res Public Health. 18(6).
10. Costa SA, Ribeiro CCC, de Oliveira KR, Alves CMC, Thomaz E, Casarin RCV, Souza SFC. 2021. Low bone mineral density is associated with severe periodontitis at the end of the second decade of life: A population-based study. J Clin Periodontol. 48(10):1322–1332.
11. Davis CA, Hitz BC, Sloan CA, Chan ET, Davidson JM, Gabdank I, Hilton JA, Jain K, Baymuradov UK, Narayanan AK et al. 2018. The encyclopedia of DNA elements (encode): Data portal update. Nucleic Acids Res. 46(D1):D794-D801.
12. DeLuca DS, Levin JZ, Sivachenko A, Fennell T, Nazaire MD, Williams C, Reich M, Winckler W, Getz G. 2012. Rna-seqc: Rna-seq metrics for quality control and process optimization. Bioinformatics. 28(11):1530–1532.
13. Descombes P, Schibler U. 1991. A liver-enriched transcriptional activator protein, lap, and a transcriptional inhibitory protein, lip, are translated from the same mrna. Cell. 67(3):569–579.

14. Dobin A, Davis CA, Schlesinger F, Drenkow J, Zaleski C, Jha S, Batut P, Chaisson M, Gingeras TR. 2013. Star: Ultrafast universal rna-seq aligner. Bioinformatics. 29(1):15–21.
15. Donham C, Chicana B, Robling AG, Mohamed A, Elizaldi S, Chi M, Freeman B, Millan A, Murugesh DK, Hum NR et al. 2021. Sclerostin depletion induces inflammation in the bone marrow of mice. Int J Mol Sci. 22(17).
16. Dror I, Golan T, Levy C, Rohs R, Mandel-Gutfreund Y. 2015. A widespread role of the motif environment in transcription factor binding across diverse protein families. Genome Res. 25(9):1268–1280.
17. ENCODE-Project-Consortium. 2012. An integrated encyclopedia of DNA elements in the human genome. Nature. 489(7414):57–74.
18. Estrada K, Styrkarsdottir U, Evangelou E, Hsu YH, Duncan EL, Ntzani EE, Oei L, Albagha OM, Amin N, Kemp JP et al. 2012. Genome-wide meta-analysis identifies 56 bone mineral density loci and reveals 14 loci associated with risk of fracture. Nat Genet. 44(5):491–501.
19. Ewels P, Magnusson M, Lundin S, Kaller M. 2016. Multiqc: Summarize analysis results for multiple tools and samples in a single report. Bioinformatics. 32(19):3047–3048.
20. Fairfield H, Rosen CJ, Reagan MR. 2017. Connecting bone and fat: The potential role for sclerostin. Curr Mol Biol Rep. 3(2):114–121.
21. Freitag-Wolf S, Munz M, Wiehe R, Junge O, Graetz C, Jockel-Schneider Y, Staufenbiel I, Bruckmann C, Lieb W, Franke A et al. 2019. Smoking modifies the genetic risk for early-onset periodontitis. J Dent Res. 98(12):1332–1339.
22. Frysz M, Gergei I, Scharnagl H, Smith GD, Zheng J, Lawlor DA, Herrmann M, Maerz W, Tobias JH. 2022. Circulating sclerostin levels are positively related to coronary artery disease severity and related risk factors. J Bone Miner Res. 37(2):273–284.
23. Garcia-Alcalde F, Okonechnikov K, Carbonell J, Cruz LM, Gotz S, Tarazona S, Dopazo J, Meyer TF, Conesa A. 2012. Qualimap: Evaluating next-generation sequencing alignment data. Bioinformatics. 28(20):2678–2679.
24. Geissler S, Textor M, Stumpp S, Seitz S, Lekaj A, Brunk S, Klaassen S, Schinke T, Klein C, Mundlos S et al. 2018. Loss of murine gfi1 causes neutropenia and induces osteoporosis depending on the pathogen load and systemic inflammation. PLoS One. 13(6):e0198510.
25. Genomes Project C, Abecasis GR, Altshuler D, Auton A, Brooks LD, Durbin RM, Gibbs RA, Hurles ME, McVean GA. 2010. A map of human genome variation from population-scale sequencing. Nature. 467(7319):1061–1073.
26. Heigwer F, Kerr G, Boutros M. 2014. E-crisp: Fast crispr target site identification. Nat Methods. 11(2):122–123.
27. Helness A, Fraszczak J, Joly-Beauparlant C, Bagci H, Trahan C, Arman K, Shooshtarizadeh P, Chen R, Ayoub M, Cote JF et al. 2021. Gfi1 tethers the nurd complex to open and transcriptionally active chromatin in myeloid progenitors. Commun Biol. 4(1):1356.

28. Hoffmann TJ, Theusch E, Haldar T, Ranatunga DK, Jorgenson E, Medina MW, Kvale MN, Kwok PY, Schaefer C, Krauss RM et al. 2018. A large electronic-health-record-based genome-wide study of serum lipids. Nat Genet. 50(3):401–413.
29. Hungness ES, Luo GJ, Pritts TA, Sun X, Robb BW, Hershko D, Hasselgren PO. 2002. Transcription factors c/ebp-beta and -delta regulate il-6 production in il-1beta-stimulated human enterocytes. J Cell Physiol. 192(1):64–70.
30. Jinesh GG, Flores ER, Brohl AS. 2018. Chromosome 19 mirna cluster and cebpb expression specifically mark and potentially drive triple negative breast cancers. PLoS One. 13(10):e0206008.
31. Kemp JP, Morris JA, Medina-Gomez C, Forgetta V, Warrington NM, Youlten SE, Zheng J, Gregson CL, Grundberg E, Trajanoska K et al. 2017. Identification of 153 new loci associated with heel bone mineral density and functional involvement of gpc6 in osteoporosis. Nat Genet. 49(10):1468–1475.
32. Kichaev G, Bhatia G, Loh PR, Gazal S, Burch K, Freund MK, Schoech A, Pasaniuc B, Price AL. 2019. Leveraging polygenic functional enrichment to improve gwas power. Am J Hum Genet. 104(1):65–75.
33. Konermann S, Brigham MD, Trevino AE, Joung J, Abudayyeh OO, Barcena C, Hsu PD, Habib N, Gootenberg JS, Nishimasu H et al. 2015. Genome-scale transcriptional activation by an engineered crispr-cas9 complex. Nature. 517(7536):583–588.
34. Lamont RJ, Koo H, Hajishengallis G. 2018. The oral microbiota: Dynamic communities and host interactions. Nat Rev Microbiol. 16(12):745–759.
35. Liberzon A, Birger C, Thorvaldsdottir H, Ghandi M, Mesirov JP, Tamayo P. 2015. The molecular signatures database (msigdb) hallmark gene set collection. Cell Syst. 1(6):417–425.
36. Love MI, Huber W, Anders S. 2014. Moderated estimation of fold change and dispersion for rna-seq data with deseq2. Genome Biol. 15(12):550.
37. Machiela MJ, Chanock SJ. 2015. Ldlink: A web-based application for exploring population-specific haplotype structure and linking correlated alleles of possible functional variants. Bioinformatics. 31(21):3555–3557.
38. Manke T, Heinig M, Vingron M. 2010. Quantifying the effect of sequence variation on regulatory interactions. Hum Mutat. 31(4):477–483.
39. Manke T, Roider HG, Vingron M. 2008. Statistical modeling of transcription factor binding affinities predicts regulatory interactions. PLoS Comput Biol. 4(3):e1000039.
40. Medina-Gomez C, Kemp JP, Trajanoska K, Luan J, Chesi A, Ahluwalia TS, Mook-Kanamori DO, Ham A, Hartwig FP, Evans DS et al. 2018. Life-course genome-wide association study meta-analysis of total body bmd and assessment of age-specific effects. Am J Hum Genet. 102(1):88–102.
41. Morris JA, Kemp JP, Youlten SE, Laurent L, Logan JG, Chai RC, Vulpescu NA, Forgetta V, Kleinman A, Mohanty ST et al. 2019. An atlas of genetic influences on osteoporosis in humans and mice. Nat Genet. 51(2):258–266.
42. Napimoga MH, Nametala C, da Silva FL, Miranda TS, Bossonaro JP, Demasi AP, Duarte PM. 2014. Involvement of the wnt-beta-catenin signalling antagonists, sclerostin and dickkopf-related protein 1,

in chronic periodontitis. J Clin Periodontol. 41(6):550–557.

43. Nielsen JB, Rom O, Surakka I, Graham SE, Zhou W, Roychowdhury T, Fritsche LG, Gagliano Taliun SA, Sidore C, Liu Y et al. 2020. Loss-of-function genomic variants highlight potential therapeutic targets for cardiovascular disease. Nat Commun. 11(1):6417.
44. Ran FA, Hsu PD, Wright J, Agarwala V, Scott DA, Zhang F. 2013. Genome engineering using the crispr-cas9 system. Nat Protoc. 8(11):2281–2308.
45. Richardson TG, Leyden GM, Wang Q, Bell JA, Elsworth B, Davey Smith G, Holmes MV. 2022. Characterising metabolomic signatures of lipid-modifying therapies through drug target mendelian randomisation. PLoS Biol. 20(2):e3001547.
46. Rueden CT, Schindelin J, Hiner MC, DeZonia BE, Walter AE, Arena ET, Eliceiri KW. 2017. Imagej2: Imagej for the next generation of scientific image data. BMC Bioinformatics. 18(1):529.
47. Sayols S, Scherzinger D, Klein H. 2016. Dupradar: A bioconductor package for the assessment of pcr artifacts in rna-seq data. BMC Bioinformatics. 17(1):428.
48. Sheng Z, Tong D, Ou Y, Zhang H, Zhang Z, Li S, Zhou J, Zhang J, Liao E. 2012. Serum sclerostin levels were positively correlated with fat mass and bone mineral density in central south chinese postmenopausal women. Clin Endocrinol (Oxf). 76(6):797–801.
49. Simeonov DR, Gowen BG, Boontanrart M, Roth TL, Gagnon JD, Mumbach MR, Satpathy AT, Lee Y, Bray NL, Chan AY et al. 2017. Discovery of stimulation-responsive immune enhancers with crispr activation. Nature. 549(7670):111–115.
50. Smink JJ, Begay V, Schoenmaker T, Sterneck E, de Vries TJ, Leutz A. 2009. Transcription factor c/ebpbeta isoform ratio regulates osteoclastogenesis through mafb. EMBO J. 28(12):1769–1781.
51. Sterken BA, Ackermann T, Muller C, Zuidhof HR, Kortman G, Hernandez-Segura A, Broekhuis M, Spierings D, Guryev V, Calkhoven CF. 2022. C/ebpbeta isoform-specific regulation of migration and invasion in triple-negative breast cancer cells. NPJ Breast Cancer. 8(1):11.
52. Styrkarsdottir U, Halldorsson BV, Gretarsdottir S, Gudbjartsson DF, Walters GB, Ingvarsson T, Jonsdottir T, Saemundsdottir J, Snorradottir S, Center JR et al. 2009. New sequence variants associated with bone mineral density. Nat Genet. 41(1):15–17.
53. Sun W, Guo J, McClellan D, Poeschla A, Bareyan D, Casey MJ, Cairns BR, Tantin D, Engel ME. 2022. Gfi1 cooperates with ikzf1/ikaros to activate gene expression in t-cell acute lymphoblastic leukemia. Mol Cancer Res. 20(4):501–514.
54. Surakka I, Fritsche LG, Zhou W, Backman J, Kosmicki JA, Lu H, Brumpton B, Nielsen JB, Gabrielsen ME, Skogholt AH et al. 2020. Mepe loss-of-function variant associates with decreased bone mineral density and increased fracture risk. Nat Commun. 11(1):4093.
55. Surakka I, Horikoshi M, Magi R, Sarin AP, Mahajan A, Lagou V, Marullo L, Ferreira T, Miraglio B, Timonen S et al. 2015. The impact of low-frequency and rare variants on lipid levels. Nat Genet. 47(6):589–597.
56. Tezal M, Wactawski-Wende J, Grossi SG, Ho AW, Dunford R, Genco RJ. 2000. The relationship between bone mineral density and periodontitis in postmenopausal women. J Periodontol.

71(9):1492–1498.

57. Thomas-Chollier M, Hufton A, Heinig M, O'Keeffe S, Masri NE, Roider HG, Manke T, Vingron M. 2011. Transcription factor binding predictions using trap for the analysis of chip-seq data and regulatory snps. Nat Protoc. 6(12):1860–1869.
58. Tominaga H, Maeda S, Hayashi M, Takeda S, Akira S, Komiya S, Nakamura T, Akiyama H, Imamura T. 2008. Ccaat/enhancer-binding protein beta promotes osteoblast differentiation by enhancing runx2 activity with atf4. Mol Biol Cell. 19(12):5373–5386.
59. van Bezooijen RL, Bronckers AL, Gortzak RA, Hogendoorn PC, van der Wee-Pals L, Balemans W, Oostenbroek HJ, Van Hul W, Hamersma H, Dikkers FG et al. 2009. Sclerostin in mineralized matrices and van buchem disease. J Dent Res. 88(6):569–574.
60. van Leeuwen EM, Sabo A, Bis JC, Huffman JE, Manichaikul A, Smith AV, Feitosa MF, Demissie S, Joshi PK, Duan Q et al. 2016. Meta-analysis of 49 549 individuals imputed with the 1000 genomes project reveals an exonic damaging variant in angptl4 determining fasting tg levels. J Med Genet. 53(7):441–449.
61. Vuckovic D, Bao EL, Akbari P, Lareau CA, Mousas A, Jiang T, Chen MH, Raffield LM, Tardaguila M, Huffman JE et al. 2020. The polygenic and monogenic basis of blood traits and diseases. Cell. 182(5):1214–1231 e1211.
62. Wehmeyer C, Frank S, Beckmann D, Bottcher M, Cromme C, Konig U, Fennen M, Held A, Paruzel P, Hartmann C et al. 2016. Sclerostin inhibition promotes tnf-dependent inflammatory joint destruction. Sci Transl Med. 8(330):330ra335.
63. Yang J, Horton JR, Akdemir KC, Li J, Huang Y, Kumar J, Blumenthal RM, Zhang X, Cheng X. 2021. Preferential cebp binding to t:G mismatches and increased c-to-t human somatic mutations. Nucleic Acids Res. 49(9):5084–5094.
64. Young MD, Wakefield MJ, Smyth GK, Oshlack A. 2010. Gene ontology analysis for rna-seq: Accounting for selection bias. Genome Biol. 11(2):R14.
65. Zeng B, Lloyd-Jones LR, Holloway A, Marigorta UM, Metspalu A, Montgomery GW, Esko T, Brigham KL, Quyyumi AA, Idaghdour Y et al. 2017. Constraints on eqtl fine mapping in the presence of multisite local regulation of gene expression. G3 (Bethesda). 7(8):2533–2544.
66. Zyla J, Marczyk M, Domaszewska T, Kaufmann SHE, Polanska J, Weiner J. 2019. Gene set enrichment for reproducible science: Comparison of cerno and eight other algorithms. Bioinformatics. 35(24):5146–5154.

Figures

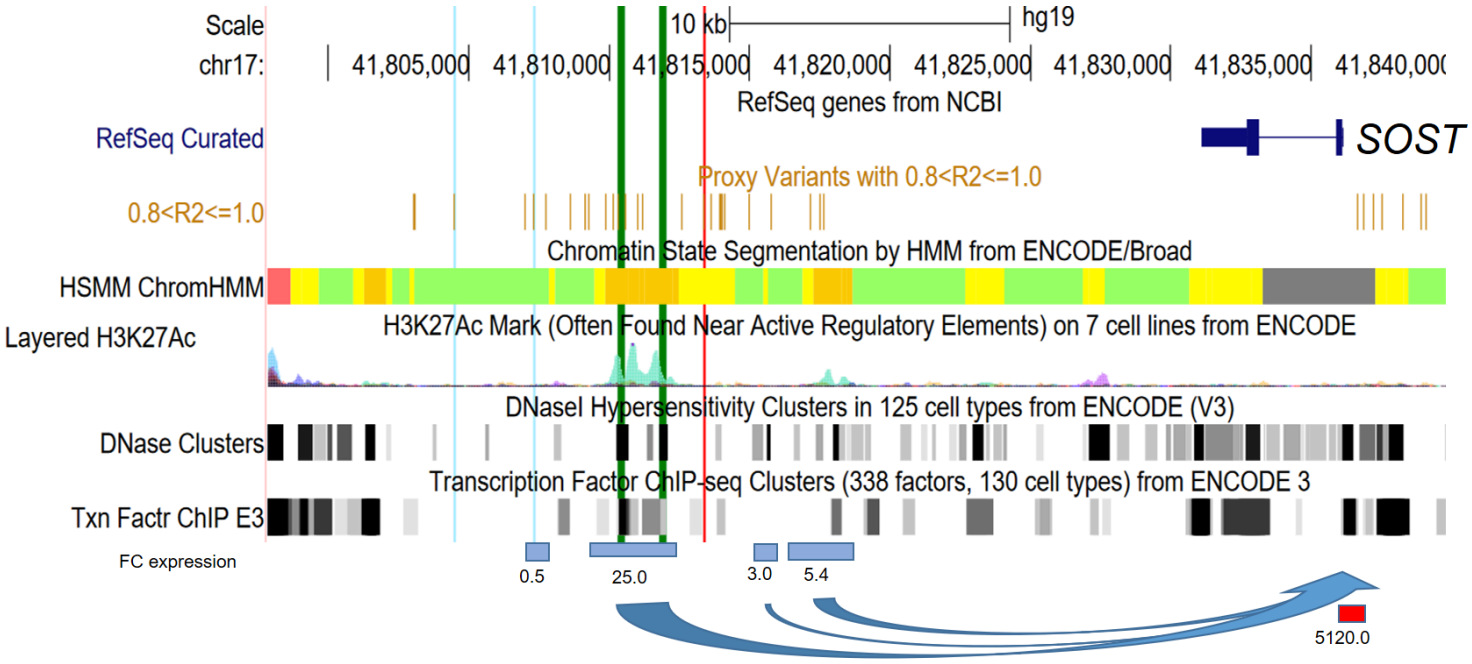

Figure 1

Overview of the genetic region associated with bone mineral density (BMD) and periodontitis at the gene *SOST*.

Cis-regulatory effects on *SOST*expression containing functional CEBPB binding sites (the order of proxy SNPs from left to right is shown in Appendix Table 1). Light blue vertical lines mark the GWAS lead SNPs rs6416905 (periodontitis, left) and rs1513670 (BMD, right). Bold green vertical lines mark the CEBPB binding sites confirmed by ChIP-Seq experiments in lung fibroblasts of Caucasian origin. A red vertical line marks the putative functional SNP rs9783823. The bottom panel shows the fold change (FC) of *SOST* expression induced by CRISPRa in the current study using sgRNAs at the positions indicated by the horizontal bars (blue bar = binding in enhancer regions, red bar = binding in promoter region). The information in the other panels was obtained from the UCSC Genome Browser (hg19) using ENCODE 3 data (color code for enhancers in the ChromHMM panel: orange = strong enhancer, yellow = weak enhancer).

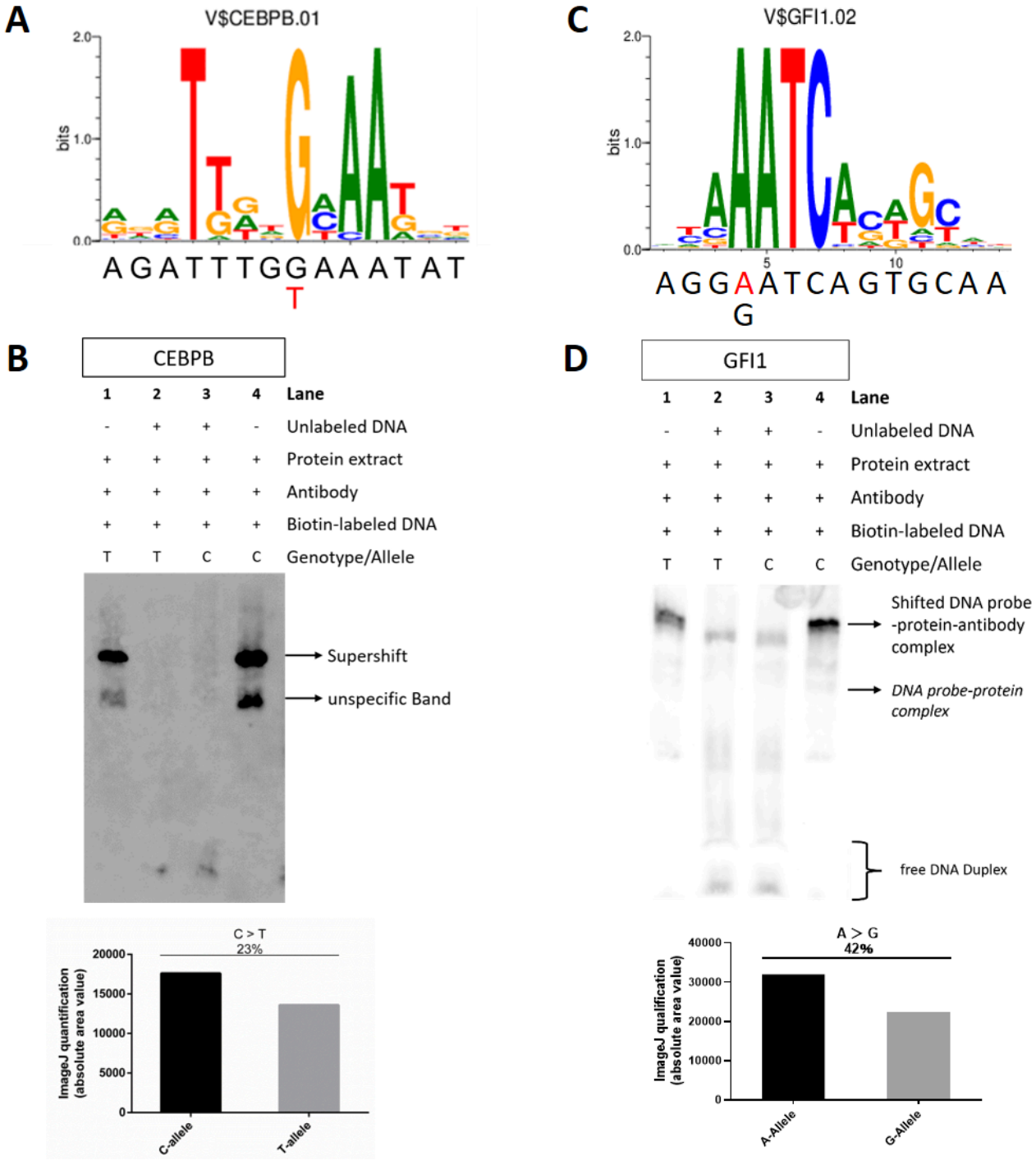

Figure 2

rs9783823-G and rs8071941-A alleles provide binding motifs for the TFs CEBPB and GFI-1.

The alternative rs9783823-T allele reduces the predicted affinity of CEBPB binding (**A**). CEBPB binding at the SNP sequence was detected by antibody EMSA, which showed a 23% reduction in CEBPB binding in the presence of the alternative T-allele (**B**). The rs8071941-G reference allele reduces the predicted affinity of GFI-1 binding (**C**), which was validated by antibody EMSA showing a 42% reduction in GFI-1 binding compared to the alternative A-allele (**D**).

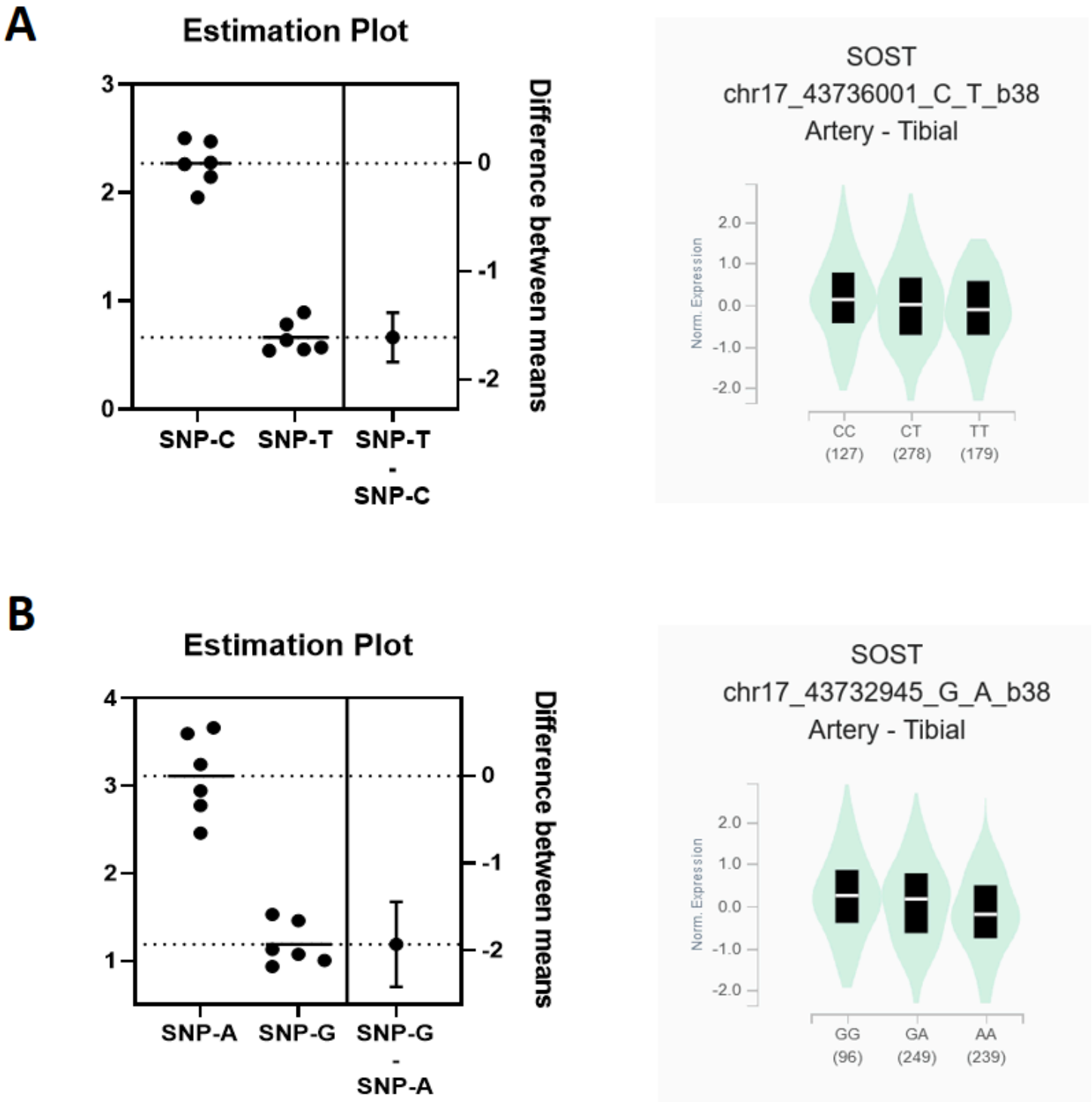

Figure 3

rs9783823 and rs8071941 have allele-specific effects on luciferase activity.

The 79 bp sequence (39 bp up-and downstream of rs9783823) increased allele-specific enhancer activity in SaOS-2 cells in the background of the C-allele (2.3-fold stronger compared to the empty plasmid (baseline 1; $P < 0.0001$) and 3.8-fold stronger compared to the T-allele ($P < 0.0001$) (**A, left panel**). GTEx observed eQTL effects of rs9783823 on *SOST* expression (tissue: artery). Consistent with the reporter

gene experiments, *SOST* expression was reduced in the background of the T-allele compared to the C-allele (normalized effect size β = -0.17, P = 5.1 x 10^{-13}; **A, right panel**). Both rs8071941 alleles increased luciferase activity (A: 3.0-fold, G: 1.3-fold, P = 0.0019; **B, left panel**). In contrast, GTEx data showed reduced *SOST* expression in the background of the A-allele (β = -0.24, P = 3.5 x 10^{-25}), consistent with the function of GFI-1 as a repressor (**B, right panel**).

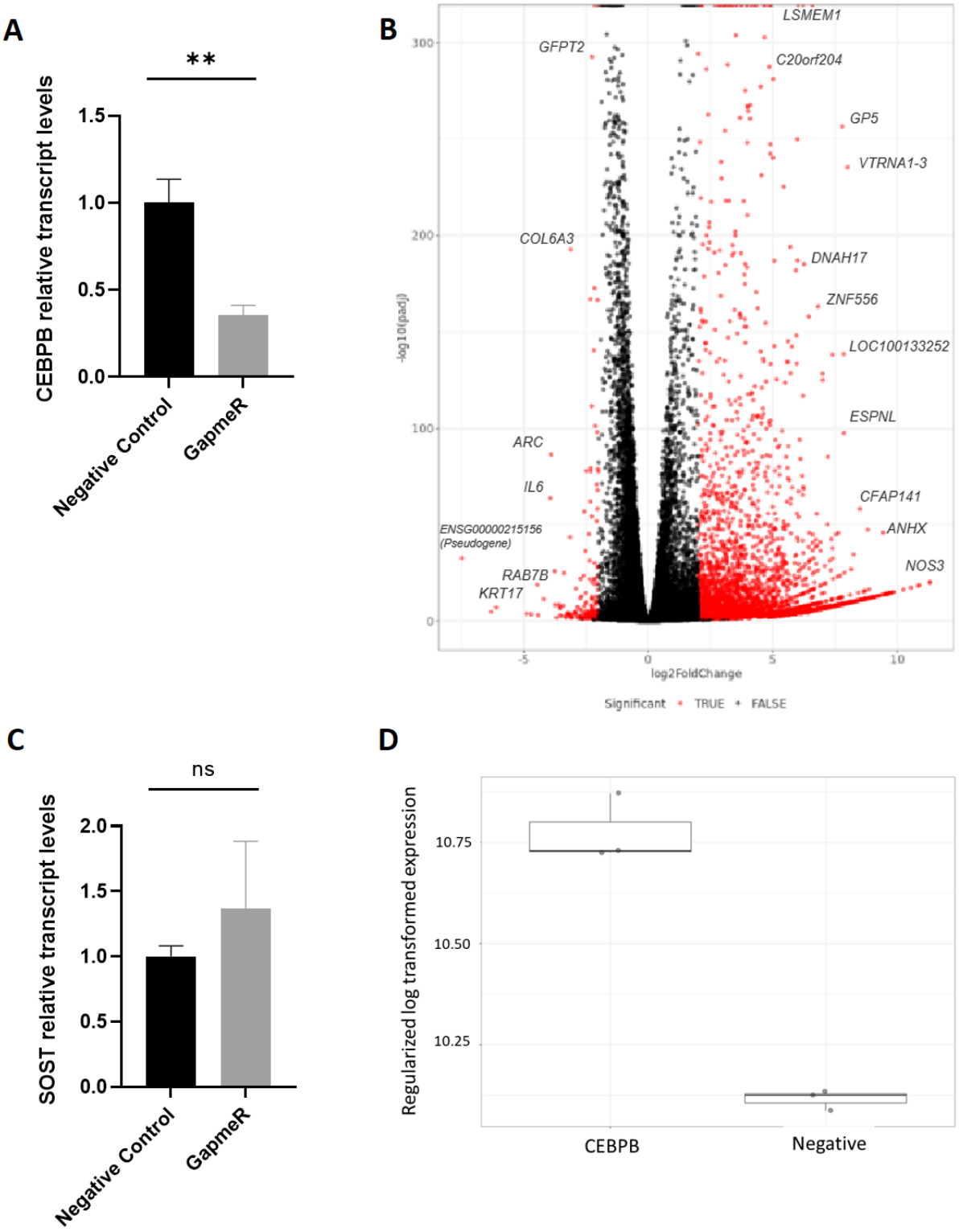

Figure 4

CEBPB knockdown for 48 h primarily induced a significant upregulation of gene expression throughout the genome.

CEBPB expression was significantly reduced (0.36-fold, P < 0.01; **A)** 48 h after LNA GapmeR transfection. Volcano plot of SaOS-2 cells after *CEBPB* knockdown primarily induced a significant upregulation of gene expression throughout the genome. Red color marks differentially expressed genes with P < 0.05 and Log2 FC > 2. The names of the most significant differentially expressed protein-coding genes are indicated (**B**). *CEBPB* knockdown in SaOS-2 cells resulted in a weak increase of *SOST* expression after 48 h. qRT-PCR with *CEBPB* specific primers (P = 0.29; **C**); RNA-Seq data (P = 4.7 x 10E-26, 0.79 log2FC; **D**).

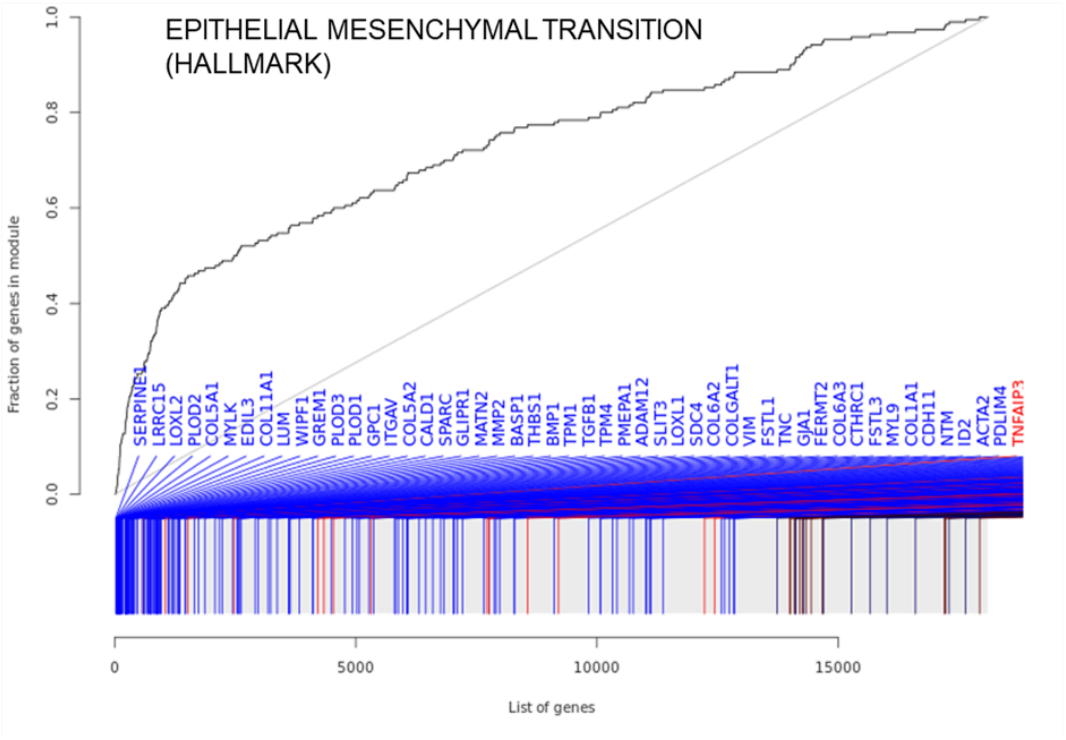

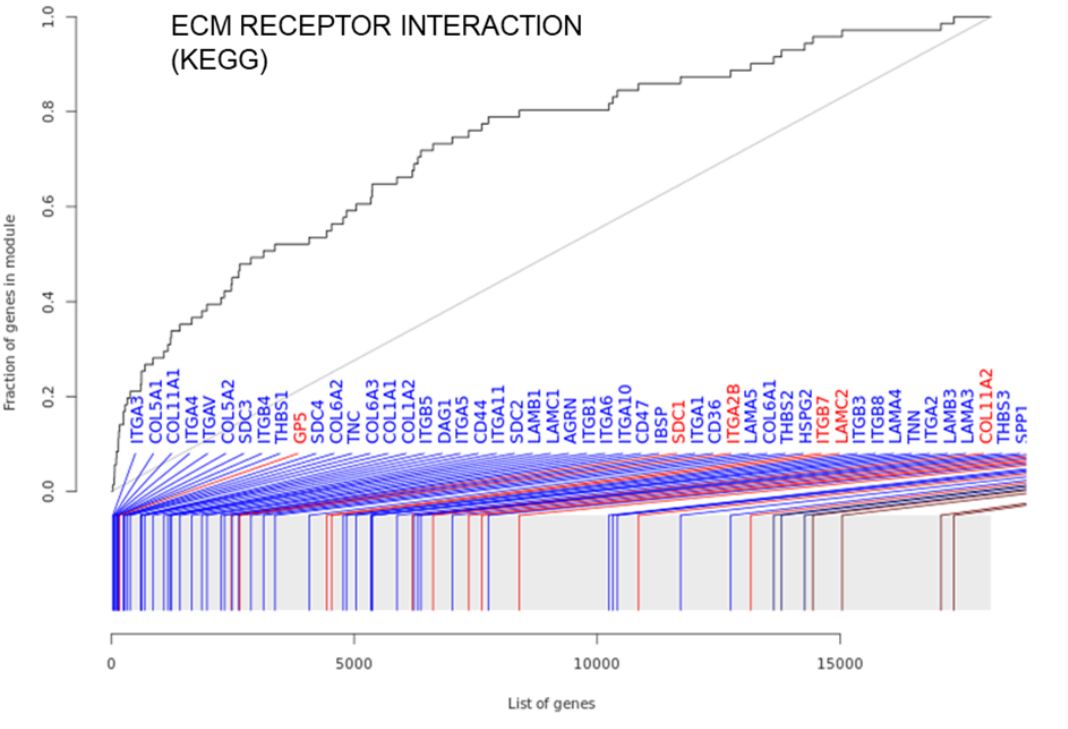

Figure 5

Most significantly enriched gene sets after *CEBPB* knockdown in SaOS-2 cells for 48 h show a role in barrier tissue remodeling.

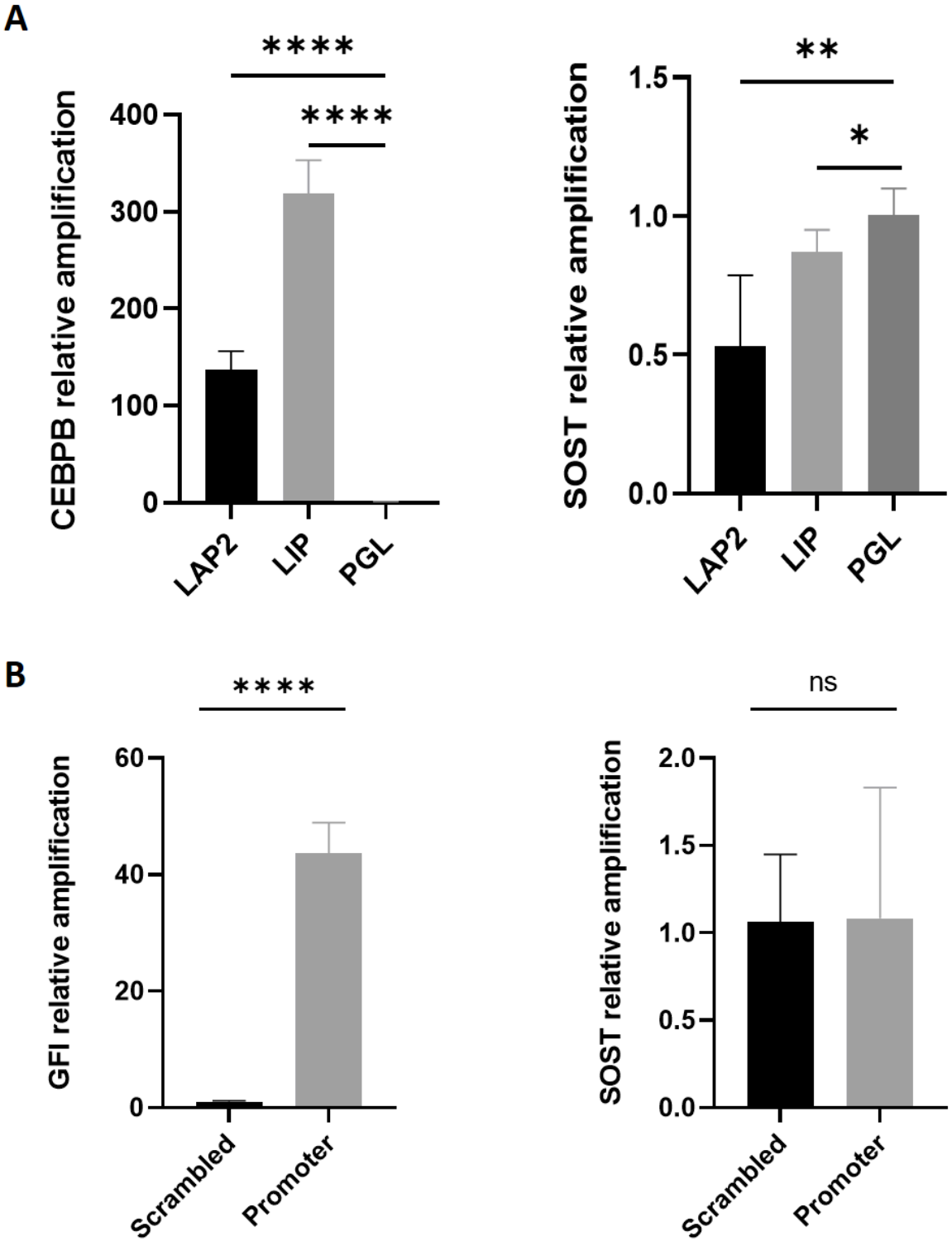

Figure 6

Effect of overexpressing *CEBPB*and *GFI-1* on *SOST* expression.

(A). Overexpression of the *CEBPB*-LAP2 isoform reduced *SOST*expression in SaOS-2 cells. Significantly increased LAP2 and LIP expression 48 h after transfection of the corresponding overexpression plasmids (**left panel**). Increased LAP2 expression correlated with weakly reduced *SOST* expression (1.89-

fold reduction, P < 0.01), and an increase in LIP expression showed a very slightly decreased *SOST*expression level (1.2-fold reduction, P < 0.05) (**right panel**)**.** PGL = negative control vector. **(B).** *GFI-1* CRISPRa did not increase *SOST*expression in Hela cells. *GFI-1* was significantly upregulated 48 h after transfection of CRISPRa plasmids with sgRNAs that targeted the GFI promoter (43-fold, P < 0.0001; **left panel**). *SOST* expression did not show corresponding changes in transcript levels (P = 0.96; **right panel**).

Supplementary Files

This is a list of supplementary files associated with this preprint. Click to download.

- SOSTAppendix.docx